Received: 22 August 2020 | Revised: 18 October 2020 | Accepted: 18 October 2020

DOI: 10.1002/pat.5159

RESEARCH ARTICLE

polymers advanced technologies WILEY

Effect of electric stimulus on human adipose-derived mesenchymal stem cells cultured in 3D-printed scaffolds

Tuba Bedir[1,2] | Songul Ulag[2,3] | Kivanc Aydogan[4] | Ali Sahin[5] | Betul Karademir Yilmaz[5] | Yahya Guvenc[6] | Michael Bozlar[7] | Cem Bulent Ustundag[1,2] | Oguzhan Gunduz[2,3]

[1]Department of Bioengineering, Faculty of Chemical and Metallurgical Engineering, Yildiz Technical University, Istanbul, Turkey

[2]Center for Nanotechnology and Biomaterials Application and Research (NBUAM), Marmara University, Istanbul, Turkey

[3]Department of Metallurgical and Materials Engineering, Faculty of Technology, Marmara University, Istanbul, Turkey

[4]Department of Electrical and Electronics Engineering, Faculty of Engineering, Marmara University, Istanbul, Turkey

[5]Department of Biochemistry, Faculty of Medicine, Marmara University, Istanbul, Turkey

[6]Department of Neurosurgery, Faculty of Medicine, Marmara University, Istanbul, Turkey

[7]School of Engineering and Applied Science, Andlinger Center of Energy and the Environment, Princeton University, Princeton, New Jersey

Correspondence
Cem Bulent Ustundag, Department of Bioengineering, Faculty of Chemical and Metallurgical Engineering, Yildiz Technical University, Istanbul 34220, Turkey.
Email: cbustundag@gmail.com

Funding information
Marmara University Scientific Research Projects Coordination Unit, Grant/Award Number: FEN-B-121218-0614

Electrical stimulation has shown great potential for nerve regeneration processes. This makes it attractive to use electrically active materials in the neural scaffold. In this paper, bismuth ferrite (BFO) nanoparticles were synthesized via co-precipitation method and incorporated to 10 wt% polylactic acid (PLA) in chloroform to obtain 3D-printed PLA/BFO biocomposites. The crystallinity of BFO nanoparticles was confirmed by XRD, and we studied its chemical structure with FTIR, as well as the mechanical properties of the 3D-printed composites. in vitro studies show that 3D-printed scaffolds have no cytotoxicity and support the proliferation of human adipose-derived mesenchymal stem cells (hADMSCs). Furthermore, 3D scaffolds embedded with BFO shows the highest cell viability relative to pristine PLA and BFO-lined PLA scaffolds. A 48 hours electrical stimulation on the hADMSC cultured inside the 3D-printed BFO-lined PLA scaffolds indicates that stimulated cells are aligned toward the BFO line. These results could indicate the potential of BFO for directing cells toward damaged tissues.

KEYWORDS
3D printing, bismuth ferrite, cell alignment, electrical stimulation, neural scaffold

1 | INTRODUCTION

Neurodegenerative diseases or physical injuries cause loss of the central nervous system (CNS) function.[1] Nerve regeneration is a challenging clinical issue due to the low regenerative capacity and complexity of the CNS.[2] Stem cell-based therapy is a promising approach in the regeneration of damaged nerves because of the proliferation and the differentiation potential of these cells under suitable conditions.[3] However, direct transplantation of stem cells has problems such as the short-time cell survivability and the limited integration with existing neural tissue.[4] The development of 3D neural scaffolds that mimic the natural extracellular matrix provides the physical support essential to direct cell growth and differentiation at the damaged site and results in better integration with the host tissue followed by new tissue development.[5]

3D printing is a rising manufacturing technology in the regenerative medicine field.[5,6] This technology allows easily controlling the

shape and structure of the scaffold and fabricating scaffolds using cells.[5] Lee et al[7] fabricated a 3D neural scaffold by combining 3D bioprinting and electrospinning techniques for the treatment of CNS diseases. This scaffold supported adhesion and proliferation of neural stem cells and increased the average neurite length and directed neurite extension.

Endogenous electric fields (EFs) have been determined and measured in different tissues and organs in vitro and in vivo.[8] Electrical treatment clinically has been performed to speed up the recovery of wounded tissues such as nerve, ligament, articular cartilage, bone, and to stimulate damaged tissues.[9,10] Electrical stimulation is also efficient in stimulating proliferation, differentiation, and migration of different cell types.[11] Previous studies reported that the electrical signal directs the migration of neural stem cells in vivo[12] and allows them to differentiate ex vivo.[13] Human mesenchymal stem cells were exposed to pulsed electromagnetic fields for one month. It demonstrated enhanced multi-lineage differentiation and proliferation potential.[14]

The use of electroactive materials in neural tissue engineering is important in terms of providing ways to apply electrical stimulation. Electroactive biomaterials ensure local electric stimulation, supply a physical template for neural cell growth and tissue repair, and allow external control over the level and duration of stimulation.[15-17] Although some electroactive materials such as polypyrrole (PPY) and polyaniline (PANI) show superior electrical properties in nerve regeneration,[18] their poor processing performance and biocompatibility have limited the widespread and effective use of these materials.[19,20] In addition, conductive scaffolds made of these polymer materials have a resistivity in the range of 1000 to 40,000 Ω cm.[19-21] This may require a greater density of electrical stimulation that can damage neural cells and tissues.[21]

Improving biocompatibility, conductivity, and mechanical strength by combining polymers with electroactive nanoparticles has been one of the most effective strategies.[22] For example, gold[23] and zinc[24] nanoparticles were used as conductive fillers due to their biocompatibility and good electrical properties to stimulate neuronal cells, thereby enhancing cell proliferation. $BiFeO_3$ (BFO), a multiferroic material, has received much attention nowadays due to the simultaneous coexistence of ferroelectricity and anti-ferromagnetism at room temperature.[25] It has an antiferromagnetic Néel temperature (T_N) of 370°C and a ferroelectric Curie temperature (T_C) of 830°C and shows rhombohedral distorted perovskite structure with space group R3c.[26] Since BFO possesses a high Neel temperature and ferroelectric transition temperature, it has the potential to be used as a filler to produce composites.[27] Dash et al incorporated the $BiFeO_3$ powders into a polyvinylidene difluoride (PVDF) polymer matrix to form the composite. BFO powders in PVDF enhanced the dielectric constant of the composite by increasing the dipole-dipole interaction between the powders.[28] In our recent study, BFO nanoparticles were added as nanofiller into polycaprolactone (PCL) scaffolds for biomedical applications. The results showed that PCL/BFO composites had greater conductivity values than pristine BFO and exhibited good biocompatibility with adenocarcinoma lung cancer cell line.[29] The superior electrical properties of BFO makes it a potential candidate for use in neural tissue engineering applications.

Directing the cells to the damaged area is a challenging process, especially for CNS injuries and diseases.[30] According to the best of our knowledge, the behavior of cells to the BFO nanoparticles on 3D-printed scaffold via electric stimulation has not been investigated. The present study makes a significant contribution to the field in terms of demonstrating the potential of BFO nanoparticles for cell directing applications in neural tissue engineering. Herein, BFO nanoparticles were produced by co-precipitation, which is a low-cost and straightforward method combined with the scaffold to direct the cells via electrical stimulation. Novel PLA scaffolds containing BFO nanoparticles were developed using 3D printing technique. PLA was preferred due to its biodegradability and forming a suitable cell environment for neural tissue engineering.[31] Human Adipose-Derived Mesenchymal Stem Cells (hADMSC) utilized to evaluate the biocompatibility of the 3D-printed scaffolds. Finally, the electric stimulation was applied to the BFO-lined PLA scaffolds cultured with hADMSC for 48 hours, and the behavior of the cells in the presence of BFO nanoparticles was examined.

2 | MATERIALS AND METHODS

2.1 | Materials

Iron (III) nitrate nonahydrate ($Fe[NO_3]_3$), Mn = 403.95 g/mol), Bismuth (III) nitrate ($Bi_5O(OH)_9(NO_3)_4$), Mn = 1.461,99 g/mol), Nitric acid (65%), and Chloroform were bought from Merck KGaA, Germany. Ammonia Solution (25%, Mn = 35.05 g/mol) was obtained from ISOLAB, Wertheim, Germany. Distilled water supplied by water distiller (Liston). Poly (L-lactic acid) (PLA, Mn = 13.000, 2003D) was purchased from Nature Works LLC, Minnetonka, MN.

2.2 | Synthesis of $BiFeO_3$ nanoparticles

Bismuth ferrite ($BiFeO_3$-BFO) nanoparticles were synthesized by co-precipitation route, which is a fast and cost-effective method. The synthesis procedure is as follows (Figure S1). 1.86 g of $Bi(NO_3)_3{\cdot}5H_2O$ and 2.58 g of $Fe(NO_3)_3{\cdot}9H_2O$ were dissolved in nitric acid (10 mL) and distilled water (10 mL), respectively. These two solutions were mixed and stirred for 15 minutes to obtain a clear mixture (Figure S1A). Then, ammonia solution was slowly added to the mixture until a pH value between 10 and 12 under stirring for co-precipitation (Figure S1B). The precipitate was filtered and washed with distilled water several times to remove undesired products (Figure S1C). Then, the particles were dried in the oven at 100°C for about 24 hours, sintered at 550°C for 3 hours, and BFO nanoparticles were obtained (Figure S1D).

2.3 | Preparation of PLA and PLA/BFO solutions

A total of 10 wt% PLA (in chloroform) was prepared as a control group by stirring for 1 hour. 0.2 g BFO (value of pH = 10.6) was added to 10 wt% PLA for 10% PLA/ 2% BFO solution and stirred for half an

hour. The prepared solutions were filled into the 10 mL syringes for 3D-printing.

2.4 | Design and 3D-printing of PLA and PLA/BFO scaffolds

Solidworks 3D CAD software was used to design the scaffolds in the dimensions of 20 mm × 20 mm × 0.1 mm. In order to adjust the printing parameters of the scaffold, the design was turned to a Stereolithography (STL) file and transferred to the software of the Ultimaker 2+ device. The modified 3D-printer (Ultimaker 2+) was used to fabricate the scaffolds. The internal properties of scaffolds were adjusted according to the following printing parameters: infill percentage: 70%, printing speed: 16.7 mm/s, nozzle diameter: 0.4 mm, extrusion width: 0.48 mm, extrusion multiplier: 4%, and at room temperature. After optimizing the printing parameters, scaffolds were printed in three different forms: 10% PLA, 10% PLA/ 2% BFO blend, and 10% PLA/2% BFO (line) as shown in Figure S2. 10% PLA scaffold as the control group, 2% BFO-blended 10% PLA scaffold for observation of BFO behavior on three dimensional-structure, and 2% BFO-lined 10% PLA scaffold for cell directing via electric stimulation were fabricated.

2.5 | Characterization of nanoparticles and 3D-printed scaffolds

The morphologies of the BFO nanoparticles and 3D-printed scaffolds were examined by a scanning electron microscope (SEM) (MA-EVO10, ZEISS). Prior to SEM analysis, samples were coated with gold for 60 seconds using Quorum SC7620. Energy-dispersive X-ray spectroscopy (EDS) of the BFO nanoparticles was examined. The size distribution of the BFO nanoparticles was characterized by dynamic light scattering (DLS) instrument (Partica SZ-100Z, USA).

Fourier Transform Infrared Spectroscopy (FTIR, JASCO-4000) was used to observe absorption bands and infrared spectra of the BFO nanoparticles and 3D-printed scaffolds. All spectra were taken in the wavelength range of 4000 to 400 cm^{-1} at 4 cm^{-1} resolution.

The thermal characteristics of the BFO nanoparticles and 3D-printed scaffolds were analyzed by a differential scanning calorimeter (DSC-60 Plus, Shimadzu, Japan). Each sample was scanned from 25°C to 600°C at a heating rate of 10°C/min under N_2 atmosphere.

The crystal structures of both nanoparticles and 3D scaffolds were characterized using X-ray diffraction (XRD) (Shimadzu-6100, Japan) with Cu-Kα radiation source (λ = 1.54060 A°). The crystallite sizes (D) of BFO nanoparticles were calculated by Debye-Scherrer formula[32]:

$$D = \frac{k.\lambda}{\beta 1/2.\cos\theta} \quad (1)$$

where, D is the average crystallite size, k is a constant (k ≈ 0.89), λ is the wavelength of the X-ray, $\beta_{1/2}$ is the full width at half maximum, and θ is the Bragg's diffraction angle.

Mechanical properties of the 3D-printed scaffolds were studied using a tensile testing machine (EZ-LX, Shimadzu, Japan) under a speed of 5 mm/min. All printed scaffolds were cut into 9 mm × 18 mm rectangular sheets and were mounted on grips at each end.

2.6 | Isolation and phenotypic characterization of hADMSC

Human subcutaneous adipose tissue was obtained from a lumbar spinal operation performed at Marmara University Pendik Education and Research Hospital (Istanbul). Marmara University Research Ethics Committee's approval (protocol number: 09.2018.679) and informed consent from patients was obtained prior to adipose tissue-derived mesenchymal stem cells isolation. Adipose tissue specimens were washed twice with phosphate-buffered saline (PBS) to remove extra blood, small vessels, and connective tissues. After digestion with 0.075% collagenase type II (Biochrom), under agitation for 60 minutes at 37°C, filtration and centrifugation at 600 rpm were performed, and the stromal vascular fraction (SVF) obtained. The supernatant was then discarded, and the cell pellet was resuspended in Dulbecco's Modified Eagle's medium (DMEM) medium (Invitrogen), supplemented with 10% fetal bovine serum (FBS; Invitrogen), and 1% antibiotic/antimycotic (Invitrogen). Culture medium was changed 48 hours after initial plating and every 3 days thereafter. hADMSCs were selected by plastic adherence and harvested (P0) 5 days after isolation at 90% confluence.

Isolated hADMSCs were characterized using cell surface markers by flow cytometry analysis. Briefly, 10,000 cultured hADMSCs at third subculture resuspended in buffer (3% BSA [bovine serum albumin]) in PBS and then appropriate fluorescein isothiocyanate (FITC), phycoerythrin (PE), and PECy5 conjugated primary antibodies for 30 minutes at 4°C. CD34-PE and CD45-PECy5 as a negative control, CD90-FITC and CD105-FITC as positive control and isotypic control were used and afterward labeled adipose tissue mesenchymal stem cells (AT-MSCs) were analyzed on a FACs Calibur Flow Cytometer (BD Biosciences).

2.7 | Culture of hADMSCs on 3D-printed scaffolds

The fabricated 3D-printed scaffolds were sterilized under Ultraviolet (UV) during the night in the 24 well plates. To provide the microenvironment to the cells, the scaffolds were incubated in DMEM growth medium supplied with 10% FBS, 0.1 mg/mL penicillin/streptomycin at 37°C, and 5% CO_2 for an hour. After incubation, the growth medium was gathered and remained medium was discarded with a micropipette. hADMSCs were seeded at a density of 50,000 cells per scaffold in the 24-well plates due to standard cell culture procedure. The same number of monolayer cells (2D) were also incubated at 37°C, 5% CO_2 for 7 days in a humidified incubator with the cell-3D scaffolds as a control group. The MTT ((3-[4,5-dimethylthiazol-2yl]-2,5-diphenyl-tetrazolium bromide))

cytotoxicity detection kit from Glentham Life Sciences was used to determine the cytotoxicity of the scaffolds at a given time interval. Elisa reader (Perkin Elmer, Enspire) was used to measure the absorbance value of the cytotoxicity test at 560 nm wavelength. To get the precise value, the assay was performed three times, and the average values of the results were taken as the mean result.

Scanning electron microscope (ZEISS, EVO MA 10) was used to observe the cellular morphology of the cells on the 3D-printed scaffolds. After 1, 3, and 7 days incubation, the growth medium was taken, and scaffolds were fixed with 4% glutaraldehyde (Sigma Aldrich). After that, scaffolds were dehydrated through serial dilutions of ethanol and dried in air. The dried scaffolds were coated with gold and examined with different magnifications by using SEM.

2.8 | Integration of the stimulation system to cell cultures

A system, which consists of silver/silver chloride (Ag/AgCl) electrodes (reference electrodes) with porous junction and cell culture microplate was established for the integration of the electrical stimulation and the cell culture scaffolds. Electrodes were used because of biocompatibility and low price. The electrodes were attached with alligator clips to connect to the stimulator outputs.

This system uses 50 mm long, 4.5 mm diameter Ag/AgCl electrodes. These are also known as RE-1S reference electrodes. The system also utilizes 16.8 mL volume, 17.4 mm depth, and 35.43 mm/34.80 mm (top/bottom) diameter wells for use as cell culture microplates. Two separate holes were made in the lid of the microplate for electrode insertion. The design of the custom-made electrical stimulation device is detailed in supporting information (Figure S3).

2.9 | Electric stimulation of hADMSCs on 3D-printed scaffolds

The experimental setup designed to investigate the effect of electrical stimulation on the hADMSC cultured on the 3D-printed BFO-lined PLA scaffold is shown in Figure S4. The BFO-lined PLA scaffolds were sterilized by immersing in 70% ethanol solution for 1 hours, followed by subjected to UV light for 24 hours. The sterilized scaffolds were fitted into 24-well plates. The hADMSCs were then seeded at a density of 5000 cells per scaffold. The cell-seeded scaffolds were incubated at 37°C with 5% CO_2 for 1 hours. When the cells showed optimal growth on the scaffolds, the scaffolds were moved to a six-well plate for electrical stimulus. One of the cultured scaffolds was used as a control group, which was not subjected to electrical stimulation. Ag/AgCl electrodes were connected to the custom-made electrical stimulation device and inserted through holes to provide electrical contact with the 3D scaffold. The BFO-lined PLA scaffold was subjected to electric stimulation (V_{pp} (peak-to-peak) = 7.96 V, I_{pp} (peak-to-peak) = 20 mA 50% duty cycle pulses with 2 Hz frequency) for 48 hours in the incubator (at 37°C with 5% CO_2).

2.10 | DAPIstaining of hADMSCs on 3D-printed scaffolds

4′,6-diamidino-2-phenylindole (DAPI) staining was performed to examine the attachment of hADMSCs on the control and stimulated scaffolds. The growth medium was removed from the plates, and scaffolds were washed with PBS. Then, all scaffolds were fixed with 4% formaldehyde for 30 minutes at room temperature, and they were washed with PBS. In the next step, 1 μg/mL DAPI (Invitrogen) was added on each scaffold to stain the nucleus of the cells and incubated for 20 minutes at room temperature. Finally, DAPI solution was removed, and scaffolds were taken to visualize under an inverted fluorescence microscope (Leica).

2.11 | Statistical analysis

The data were normally distributed and were expressed as M ± SD of the mean. Differences between the groups were determined by one-way analysis of variance (ANOVA) with Tukey-Kramer Multiple Comparisons Test. A *P*-value of less than .05 has been accepted to be statistically significant.

3 | RESULTS AND DISCUSSION

3.1 | Characterization of BFO nanoparticles and 3D-printed scaffolds

SEM image and EDS analysis of bismuth ferrite nanoparticles produced by co-precipitation method are shown in Figure 1. As can be seen from Figure 1A, $BiFeO_3$ nanoparticles display a relatively uniform size distribution. According to EDS analysis, bismuth is found to be 71.5 wt% and iron 10 wt% in all particles, and no impurities were observed (Figure 1B). DLS measurements indicated that the mean size of the BFO nanoparticles is 144 nm (Figure S5).

Figure 2 illustrates SEM images and pore size distributions of 3D-printed scaffolds. SEM images show that pristine PLA, PLA/BFO blend, and PLA/BFO (line) scaffolds have uniform morphology with micrometer resolution channels. As shown in Figure 2A, PLA scaffold as the control group exhibits square pore shape, and its average pore size is about 294 μm (Figure 2B). In Figure 2C, BFO-blended PLA scaffold has regular pore shape and 285 μm average pore size (Figure 2D). There are no significant differences in point of morphology and surface texture between PLA and PLA/BFO scaffolds, however, PLA/BFO blend has a rougher surface that represents the existence of BFO.[33] BFO-lined PLA scaffold has also uniform pore shape, as seen in Figure 2E and its average pore size is about 241 μm

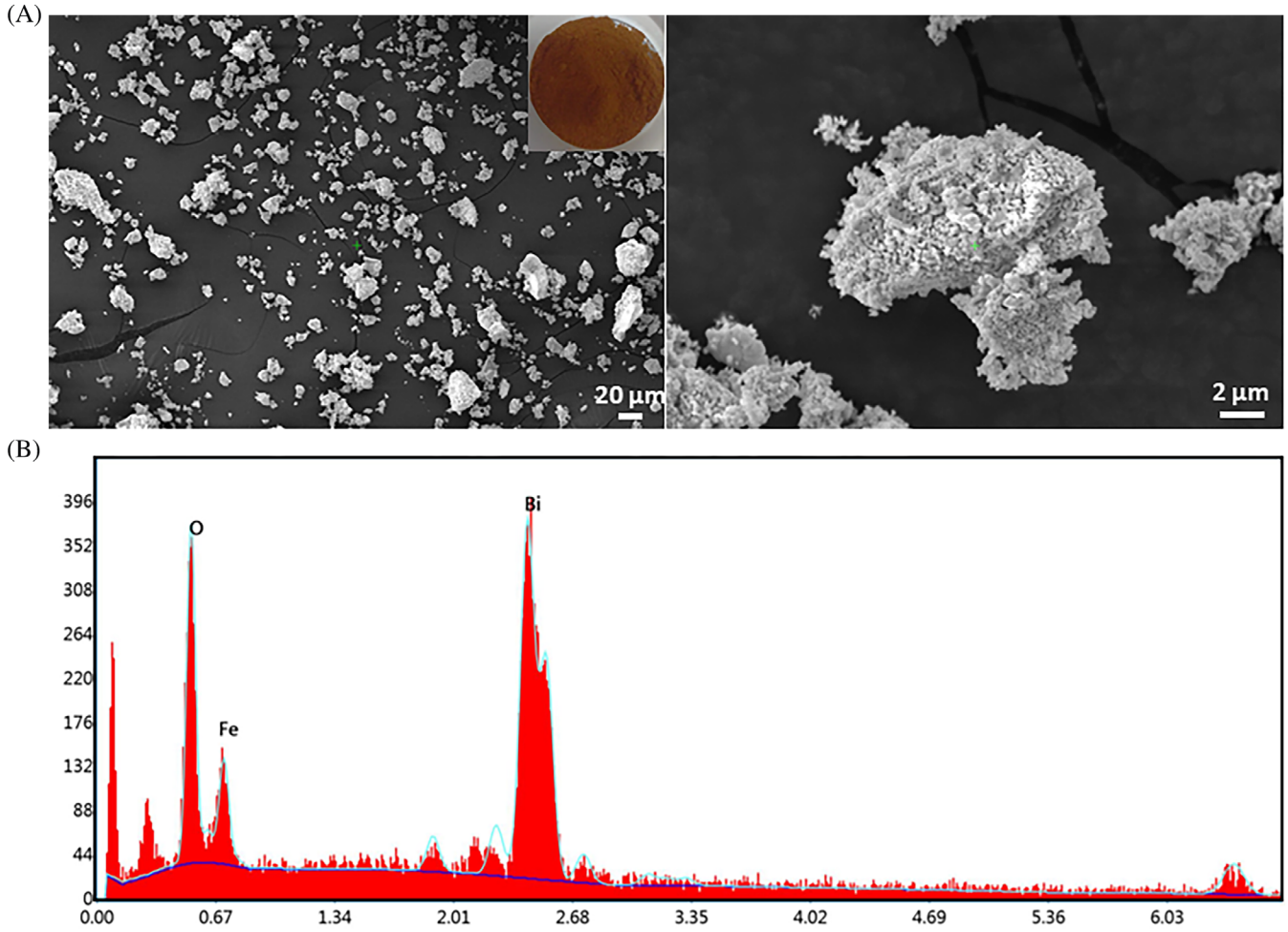

FIGURE 1 SEM images (A) and EDS analysis (B) of bismuth ferrite nanoparticles

(Figure 2F). The only difference of this scaffold from the PLA scaffold morphologically is that it contains a 300 µm thickness of BFO line in the middle. According to these, 3D printing permits the fabrication of scaffolds with desired pore geometry and pore size.[34]

Figure 3A displays the FTIR spectra of BFO nanoparticles and 3D-printed scaffolds. In Figure 3A(a), for BFO, the band at around 2369 cm^{-1} was due to the presence of atmospheric carbon dioxide in sample.[35] The peaks at positions of around 810 and 1388 cm^{-1} reveal the existence of trapped nitrates.[26] Specifically, two strong absorption peaks at around 450 and 525 cm^{-1} are attributed to the modes of Fe—O stretching vibrations and O—Fe—O bending vibrations, which are characteristics of the octahedral FeO_6 groups in the perovskites. The existence of metal-oxygen band supports the formation of perovskite structure in BFO.[36] Figure 3A(b-d) shows the absorption peaks of PLA, PLA/BFO blend, and PLA/BFO (line) scaffolds, respectively. The characteristic peaks for pristine PLA are appeared at around 1748 (C═O stretching), 1452 (—CH_3 asymmetric deformation), 1180 (C—O—C stretching), 1042 (C—CH_3 stretching), and 867 cm^{-1} (C—COO stretching).[37] By the addition of BFO, slight shifts in the position of the PLA peaks are observed. These results indicate that the BFO is successfully dispersed in PLA solutions.

DSC curve of the BFO nanoparticles prepared by co-precipitation process with 550°C is shown in Figure 3B(a). The exothermic peak at around 285°C is attributed to the Bi_2O_3 and Fe_2O_3 phases formation. In addition, the mass loss owing to the decomposition of $Bi(OH)_3$ and $Fe(OH)_3$ into a metastable phase corresponds to this peak.[38,39] Figure 3B(b-d) shows the DSC curves for PLA, PLA/BFO blend, and PLA/BFO (line) scaffolds. In Figure 3B(c), pristine PLA displays an endothermic peak of melting temperature, Tm = 158°C.[40] No changes in Tm values are seen for PLA composites because the addition of BFO did not significantly affect the Tm of PLA. The exothermic peak at around 100.5°C is observed due to the cold crystallization process for pristine PLA. In Figure 3B(d), after blending BFO nanoparticles to PLA, the cold crystallization temperature (Tcc) is shifted to the higher temperature. This means that the BFO content causes a stronger inhibition for the cold crystallization process.[41] Since the amount of PLA is more dominant, no significant change is observed in the Tcc of the BFO-lined PLA (Figure 3B[b]).

In order to determine the crystal structures of BFO powders and 3D-printed scaffolds, XRD is performed. Figure 3C shows the diffraction patterns of the BFO nanoparticles, PLA, PLA/BFO blend, and PLA/BFO (line) scaffolds. In Figure 3C(a), BFO has main sharp

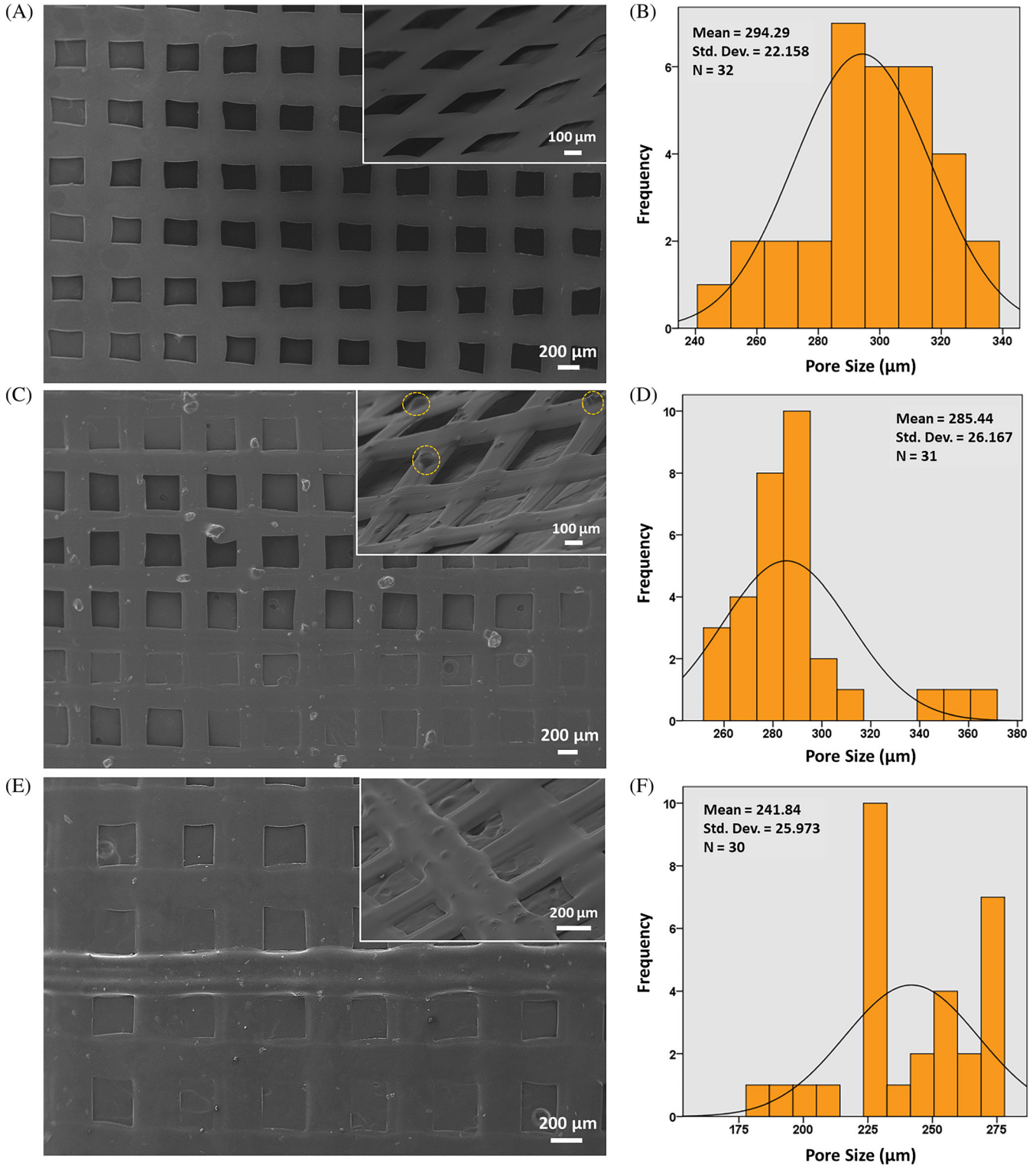

FIGURE 2 SEM images and pore size distributions of 3D-printed PLA (A, B), PLA/BFO (C, D), PLA/BFO (line) (E, F) scaffolds. The inset images correspond to the cross-sections of the samples, and the BFO aggregates inside the PLA/BFO composites are highlighted with the yellow circles

diffraction peaks at 2θ = 22.5°, 32°, 38°, 45°, 52°, 56°, 64°, and 78°. These sharp peaks promote the degree of the crystallinity of the synthesized BFO nanoparticles.[42] All peaks could be identified as rhombohedral distorted perovskite structure of bismuth ferrite with R3c space group.[43] The average crystallite size of the BFO is evaluated by Scherrer formula from XRD peak with the highest intensity

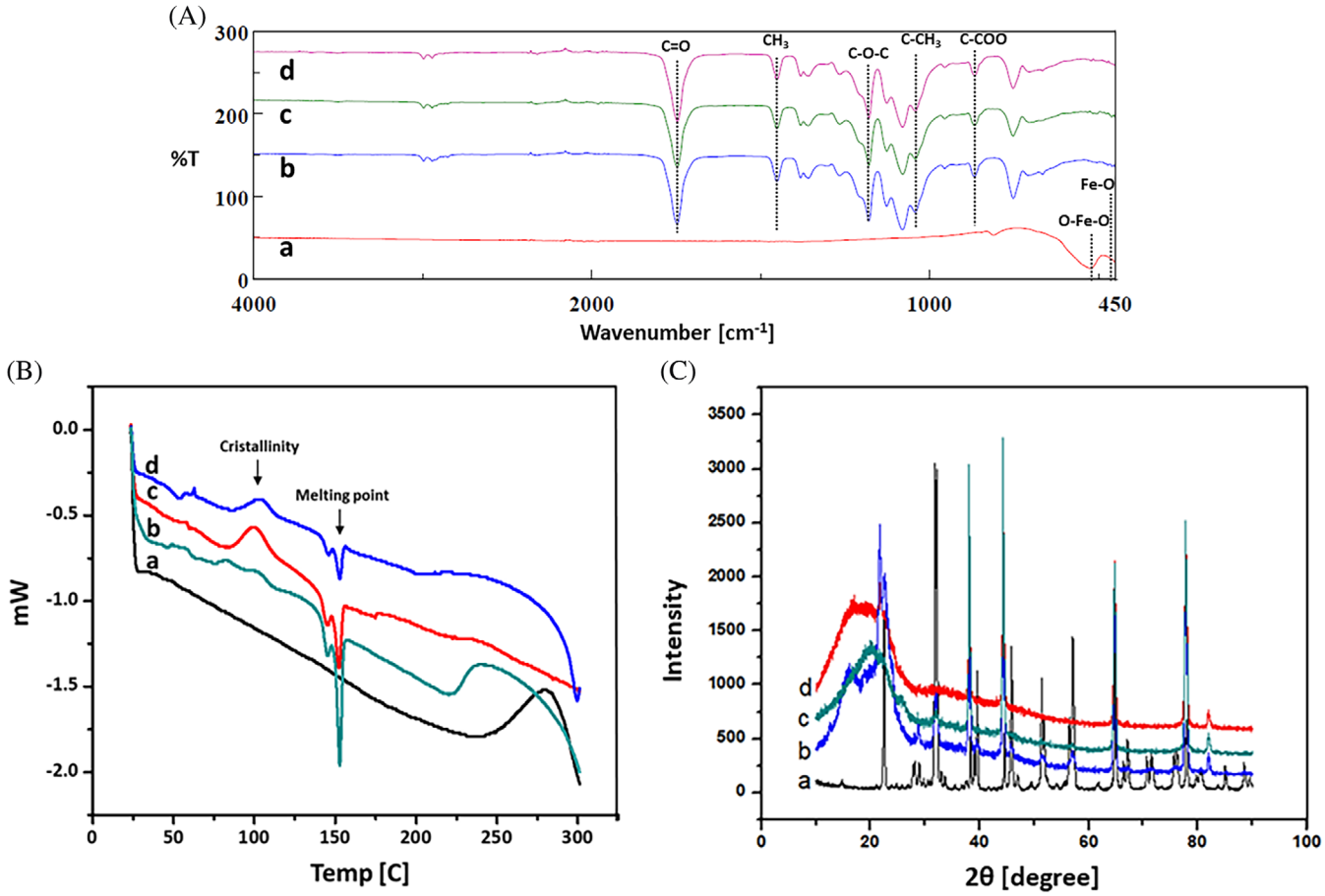

FIGURE 3 (A) FTIR spectra of the BFO nanoparticles and 3D-printed scaffolds: BFO (a), PLA (b), PLA/BFO blend (c), and PLA/BFO (line) (d). (B) DSC curves of the BFO nanoparticles and 3D-printed scaffolds: BFO (a), PLA (c), PLA/BFO blend (d), and PLA/BFO (line) (b). (C) XRD spectra of the BFO nanoparticles and 3Dprinted scaffolds: BFO (a), PLA (d), PLA/BFO blend (b), and PLA/BFO (line) (c)

and found as around 15 nm, which is the range between nanometers. The average particle size (144 nm) determined from DLS is greater than the particle crystallite size obtained from the XRD pattern. This difference could be due to the agglomeration of the BFO nanoparticles.[44] The sharp peak with low intensity is observed at 2θ = 22, 62, 78, 82° for PLA (Figure 3C[d]). The broad peak at $2\theta \approx 16°$ is the characteristic peak of the PLA and indicates the amorphous structure of it.[45] This amorphous curve points to the low degree of crystallinity of PLA scaffold.[46] The XRD pattern of the PLA/BFO blend has all diffraction peaks of the BFO nanoparticles and two characteristic peaks of PLA: A sharp peak observed at around 15° and a small peak, which showed low-intensity at around 83° (Figure 3C[b]). The observation of both BFO and PLA peaks in the blends indicated that homogeneous mixtures are obtained effectively. In Figure 3C(c) for the scaffold of PLA/BFO (line), there are obtained nearly all peaks of BFO and two characteristic peaks of PLA with low (83°) and high (18°) intensity values. The diffraction peak of PLA is shifted from 16° to 18° by the addition of the BFO line. It can be concluded from the spectra that PLA has an amorphous structure. However, the addition of the crystalline BFO powder, shows semi-crystalline structures, which contains both amorphous and crystalline domains.[47]

The tensile properties of 3D-printed scaffolds are shown in Figure 4 and summarized in Table S1. The experimental measurements indicate that the PLA/BFO composites have lower moduli than the pristine PLA. This is an unexpected observation as the addition of stiff BFO nanoparticles into the PLA matrix should have increased the modulus of the composites. Indeed, BFO nanoparticles have about at least three orders of magnitude larger Young's modulus than the PLA matrix. Possible explanations for the lower moduli in the case of composites are the altered chemistry of the PLA matrix in the presence of BFO particles. The decrease in Young's modulus of PLA composites indicates the formation of voids around PLA due to poor bonding between the BFO particles and PLA matrix in the absence of interfacial adhesion. However, BFO tends to agglomerate presumably due to van der Waals forces, which also results in weak interfacial bonding between PLA and BFO.[48] The results also indicate that the BFO based composites have a much lower elongation at break (about 50% less than pristine PLA), which is accompanied by lower tensile strength than pristine PLA. Such an observation is attributed to: (a) the

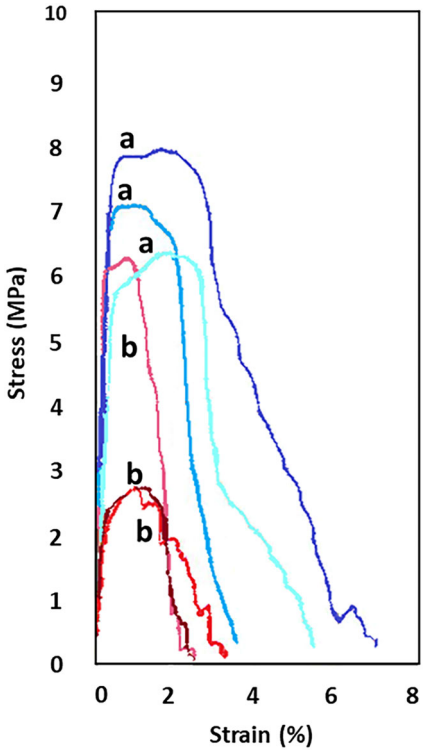

FIGURE 4 Stress-strain curves of 3D-printed PLA (a) and PLA/BFO blend (b) scaffolds

presence of defects as a result of the aggregation of BFO particles revealed by the SEM analysis carried out on cross-sections of PLA/BFO composites, which is evidenced through the lower elongation at break of solid composites compared to pristine PLA, (b) the synergy between low Young's modulus and insufficient elongation at break, which results in low strength. Surface modification of BFO can enhance adhesion both BFO, and PLA matrices, thus higher mechanical performance of the composite can be obtained.[49]

3.2 | Phenotypic characterization of subcutaneous hADMSCs

The mesenchymal nature of the isolated hADMSCs was confirmed before creating the scaffolds. Flow cytometry analysis resulted that subcutaneous hADMSCs expressed a low percentage of CD34 and CD45 while the typical surface markers of stem cells, CD90 and CD105 were highly expressed in hADMSCs, showing to meet the standards established by the International Society for Cellular Therapy (Figure S6).[50]

3.3 | Cytocompatibility of the 3D-printed scaffolds

The cell viability of hADMSCs in the presence of PLA and PLA/BFO scaffolds has been examined by 3-(4,5-dimethylthiazol-2-yl)-2,5-diphenyltetrazolium bromide (MTT) assay. Figure 5 demonstrates the MTT absorption values for hADMSCs cultured in the cell culture plate with scaffolds during the incubation period (1, 3, and 7 days). It is clearly shown that in vitro examination with hADMSCs demonstrated no cytotoxic effect, and it can be said that scaffolds can be an excellent material to seed the cells. During the first day of incubation, it is observed that cell viability values for all scaffolds were decreased compared to the 2D cell line. This can be due to the dead cells on the scaffolds.[51] Maximum viability value (71%) observed for PLA scaffolds and PLA/BFO (line) has the lowest value (57%). The columns showed a steady increase in cell viability values on PLA and PLA/BFO scaffolds from day 3 and 7. On day 3, the cell viability on the scaffolds increased substantially. The maximum increase observed for PLA/BFO blend, which is 132%. After 7 days of cell culture, the viability of cells incubated with PLA scaffolds is 113%. Scaffolds blended with BFO exhibit the highest viability (129%) results compared with the control (2D), pristine PLA and PLA/BFO (line). The contact angle of PLA is 74.3 ± 11.0°, which relatively corresponds to hydrophobic surface.[52] The roughness of a hydrophobic surface affects cell spreading and proliferation and reduces both cellular activities with materials owning larger contact angles.[53] It is thought that the addition of BFO to PLA makes the surface of the scaffold rougher than the naive PLA. Thus, hADMSCs can better adhere and proliferate on the BFO blended PLA scaffolds due to rough surface. However, it was observed that all the scaffolds could be an excellent candidate to proliferate the hADMSCs.

3.4 | hADMSC adhesion and its 3D morphology on the 3D-printed scaffolds

The cell-surrounding environment is an essential parameter for different cell actions.[54] The morphology and attachment of hADMSCs on the scaffolds were determined by SEM imaging. On the 7th day of cell culture, the hADMSCs were attached on scaffolds and showed a specific spindle-shaped morphology (Figure 6). In Figure 6A, PLA scaffolds cultured with hADMSCs demonstrate significant microenvironment for cells. The cells grew on scaffolds and showed an apparent three-dimensional morphology with partial cell-cell interactions.[55] In Figure 6B,C, cells on composites show more significant spreading morphology compared to the pristine PLA scaffold. This spreading morphology is a characteristic network-like structure of fibroblastic tissue.[56] The extracellular matrix can be associated with this network structure. In Figure 6b, the cells on PLA/BFO blends show spread morphology with broadening cytoplasmic protrusions and multiple filopodia after cell seeding.[57] The SEM images of PLA/BFO (line) have more loaded cells, and cell morphologies with cell-cell contacts are seen exactly (Figure 6C). It is known that the changes in cell morphology indicate cell activity, and this promoted the cellular migration behavior of the cells.[58] As a result, it can be concluded from the images that the observed strong adhesion and proliferation promoted the biocompatibility of all scaffolds. Besides, more cell density near the BFO line and cell-cell contact on the PLA/BFO (line) scaffold showed the BFO effect on the cell direction.

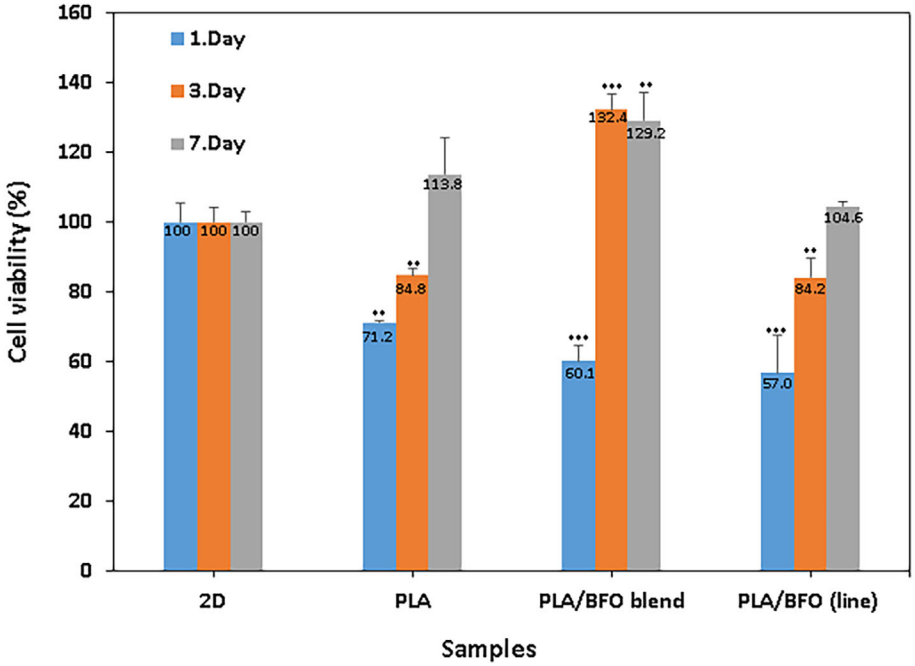

FIGURE 5 MTT assay results of hADMSCs on 3D-printed PLA, PLA/BFO blend, and PLA/BFO (line) scaffolds. $^{**}P < .01$, $^{***}P < .001$

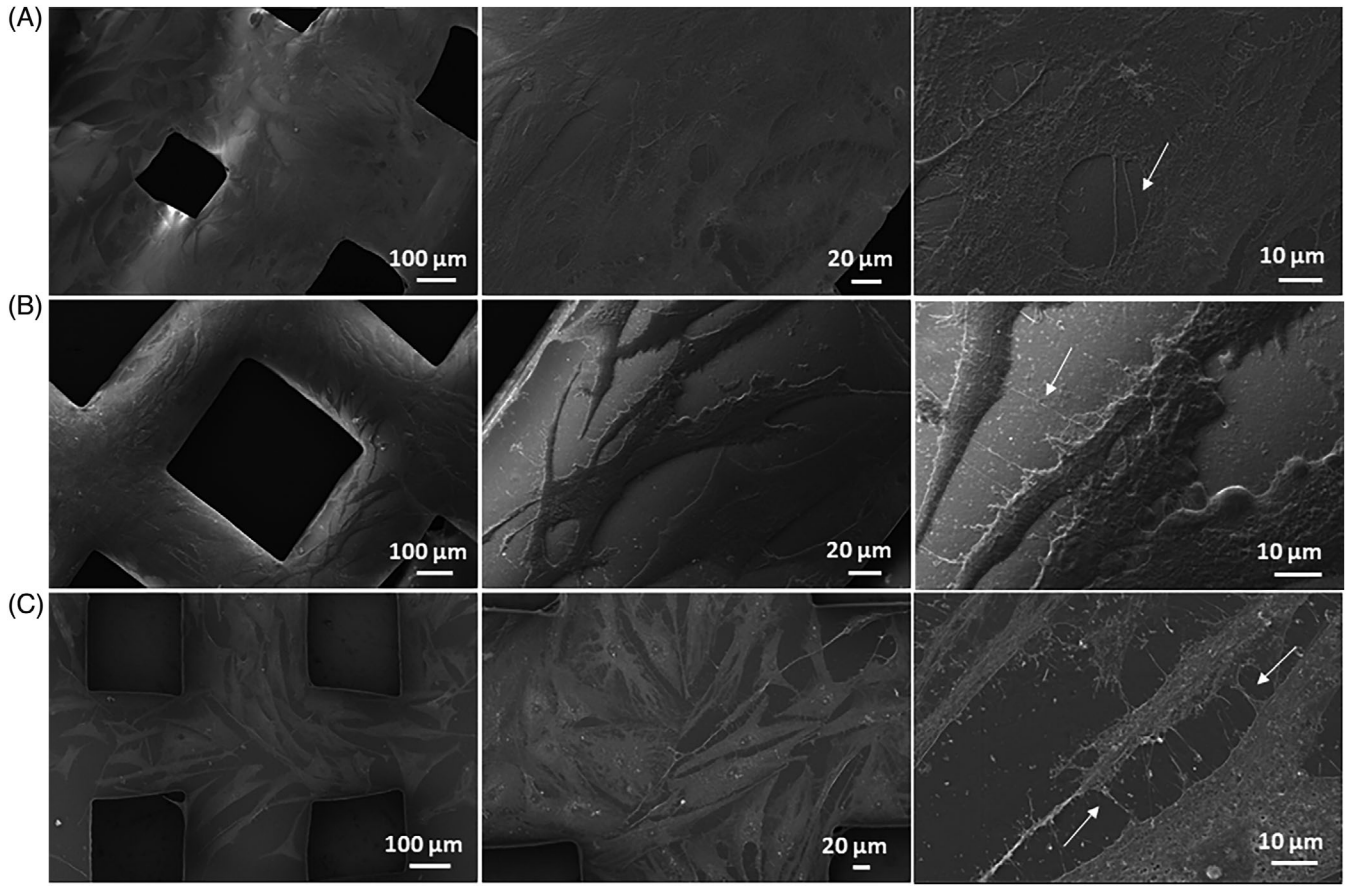

FIGURE 6 SEM images of the cultured 3D-printed scaffolds on the seventh day of cell growth: PLA (A), PLA/BFO blend (B), PLA/BFO (line) (C)

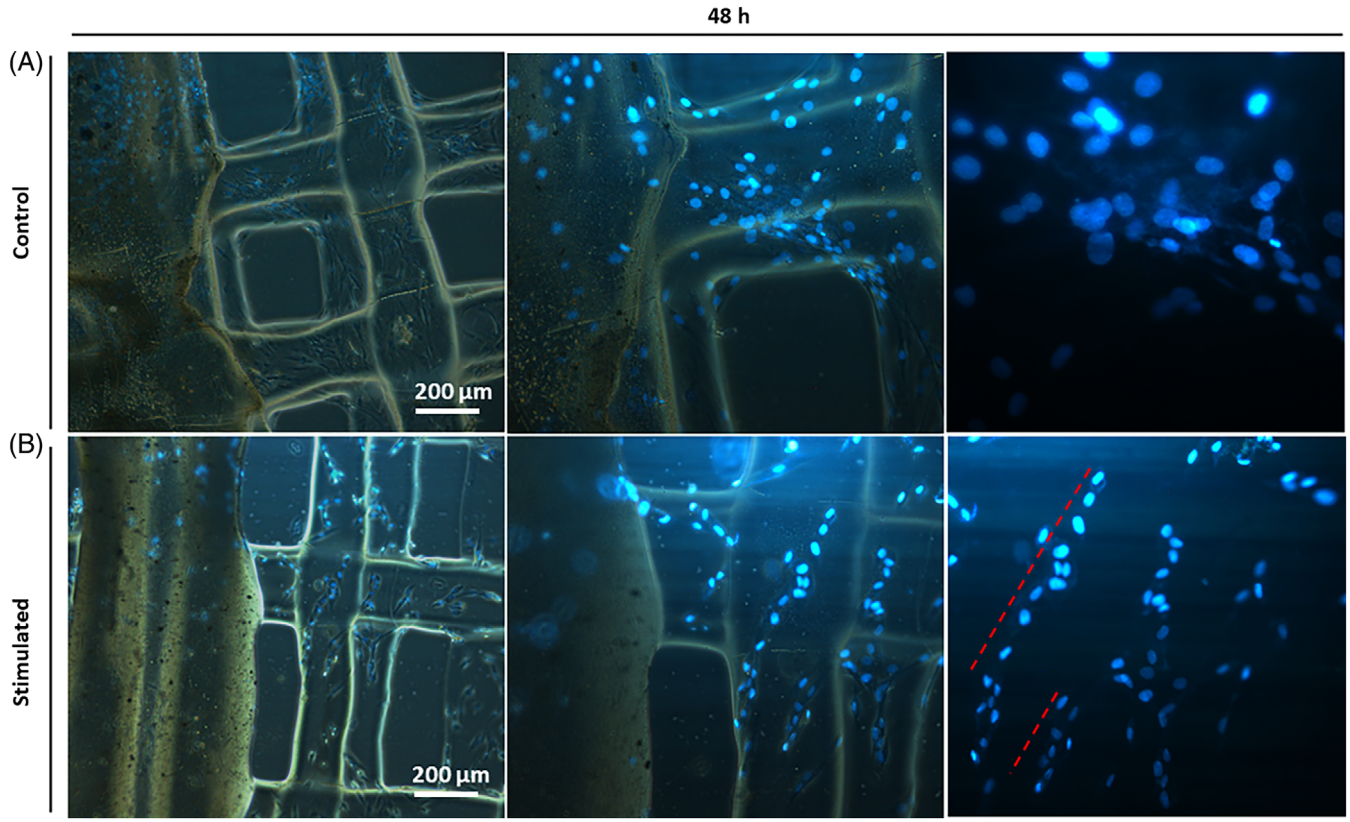

FIGURE 7 Fluorescence microscopy images of control (unstimulated) and stimulated PLA/BFO (line) scaffolds for 48 h. The line on stimulated scaffold indicate alignment of cells

3.5 | Electric stimulation of hADMSCs on 3D-printed scaffolds

Electrical stimulation was applied on 3D-printed BFO-lined PLA scaffold cultured with hADMSC. BFO-lined PLA scaffold was preferred to carry the electrical stimulus locally. As stated in the experimental section, the scaffold was exposed to electric stimulation (V_{pp} = 7.96 V, I_{pp} = 20 mA 50% duty cycle pulses with 2 Hz frequency) for 48 hours. Previous studies showed that the electrical stimulation in the range of 1 to 10 V/cm, which is above the physiological level, thereby increases the migration rate of human BMSCs.[59]

In Figure 7, fluorescence microscopy images for 48 hours clearly show that the cells in the control group are distributed randomly (Figure 7A), and the stimulated cells are aligned toward the BFO line (Figure 7B). Alignment of the cells appears more evident at high magnification. This demonstrates that electric stimulation has a significant influence on cell alignment and redirects random cells to be aligned.[60,61] In addition, the presence of BFO nanoparticles may have the potential to direct the transplanted cells to the lesion sites for the repair of neural tissue.

4 | CONCLUSIONS

The BFO nanoparticles were successfully prepared via co-precipitation route and incorporated into the PLA scaffold to direct the cells locally. PLA, PLA/BFO, and PLA/BFO (line) neural scaffolds were fabricated by a 3D printing method in the desired pore size and geometry. XRD results supported the characteristic crystal structure of the BFO and existence of interactions between BFO and PLA. Average crystalline size of BFO was found to be 15 nm, which is calculated from Scherrer formula applied to XRD spectra. According to in vitro studies, all 3D-printed scaffolds exhibited no cytotoxic effect and supported the proliferation of hADMSCs. Furthermore, the highest cell viability was observed on the 3D-printed scaffold blended with BFO. More importantly, as the BFO-lined scaffold was subjected to electrical stimulation for 48 hours, the cells in the control group were randomly distributed while the cells in the stimulated scaffold were aligned toward the BFO line. This is important in directing the cells to the damaged area to treat nervous system disorders. The present study demonstrates the potential of BFO nanoparticles on the directing of cells with the effect of electrical stimulation. However, further studies are required using specific cell differentiation markers to differentiate mesenchymal stem cells into neural tissue.

ACKNOWLEDGEMENT

This work has been supported by Marmara University Scientific Research Projects Coordination Unit under grant number FEN-B-121218-0614.

SUPPORTING INFORMATION

The following files are available free of charge: Designing of electrical stimulation device; Tensile properties of 3D-printed scaffolds; Schematic

illustration of the preparation of $BiFeO_3$ nanoparticles by co-precipitation route; 3D printing process; The comprehensive circuit diagram of the bi-channel electrical stimulation device; Cell culture microplate with Ag/AgCl electrodes inserted for electrical stimulation (a), a schematic diagram of the entire electrical stimulation system (b); Size characterization of BFO nanoparticles by DLS; The immunophenotype of hADMSCs.

ORCID

Ali Sahin https://orcid.org/0000-0001-5594-1551
Cem Bulent Ustundag https://orcid.org/0000-0002-4439-0878

REFERENCES

1. Imamura Y, Mukohara T, Shimono Y, et al. Comparison of 2D- and 3D-culture models as drug-testing platforms in breast cancer. *Oncol Rep*. 2015;33(4):1837-1843. https://doi.org/10.3892/or.2015.3767.
2. Gurgo RD, Bedi KS, Nurcombe V. Current concepts in central nervous system regeneration. *J Clin Neurosci*. 2002;9(6):613-617. https://doi.org/10.1054/jocn.2002.1080.
3. Haston KM, Finkbeiner S. Clinical trials in a dish: the potential of pluripotent stem cells to develop therapies for neurodegenerative diseases. *Annu Rev Pharmacol Toxicol*. 2016;56(1):489-510. https://doi.org/10.1146/annurev-pharmtox-010715-103548.
4. Ronaghi M, Erceg S, Moreno-Manzano V, Stojkovic M. Challenges of stem cell therapy for spinal cord injury: human embryonic stem cells, endogenous neural stem cells, or induced pluripotent stem cells? *Stem Cells*. 2010;28(1):93-99. https://doi.org/10.1002/stem.253.
5. Bedir T, Ulag S, Ustundag CB, Gunduz O. 3D bioprinting applications in neural tissue engineering for spinal cord injury repair. *Mater Sci Eng C*. 2020;110:110741. https://doi.org/10.1016/j.msec.2020.110741.
6. Hacıoglu A, Yılmazer H, Ustundag CB. 3D Printing for Tissue Engineering Applications. *J Polytech*. 2018;0900(1):221-227. https://doi.org/10.2339/politeknik.389596.
7. Lee SJ, Nowicki M, Harris B, Zhang LG. Fabrication of a Highly Aligned Neural Scaffold via a Table Top Stereolithography 3D Printing and Electrospinning. *Tissue Eng-Part A*. 2017;23(11–12):491-502. https://doi.org/10.1089/ten.tea.2016.0353.
8. Levin MH, Jung KK, Hu J, Verkman AS. Potential difference measurements of ocular surface Na+ absorption analyzed using an electrokinetic model. *Investig Ophthalmol Vis Sci*. 2006;47(1):306-316. https://doi.org/10.1167/iovs.05-1082.
9. Kim KM, Croy T, Hertel J, Saliba S. Effects of neuromuscular electrical stimulation after anterior cruciate ligament reconstruction on quadriceps strength, function, and patient-oriented outcomes: a systematic review. *J Orthop Sports Phys Ther*. 2010;40(7):383-391. https://doi.org/10.2519/jospt.2010.3184.
10. Willand MP. Electrical stimulation enhances reinnervation after nerve injury. *Eur J Transl Myol*. 2015;25(4):243-248. https://doi.org/10.4081/ejtm.2015.5243.
11. Chang KA, Kim JW, Kim JA, et al. Biphasic electrical currents stimulation promotes both proliferation and differentiation of fetal neural stem cells. *PLoS One*. 2011;6(4):e18738. https://doi.org/10.1371/journal.pone.0018738.
12. Cao L, Wei D, Reid B, et al. Endogenous electric currents might guide rostral migration of neuroblasts. *EMBO Rep*. 2013;14(2):184-190. https://doi.org/10.1038/embor.2012.215.
13. Li L, El-Hayek YH, Liu B, et al. Direct-Current Electrical Field Guides Neuronal Stem/Progenitor Cell Migration. *Stem Cells*. 2008;26(8):2193-2200. https://doi.org/10.1634/stemcells.2007-1022.
14. Hronik-Tupaj M, Rice WL, Cronin-Golomb M, Kaplan DL, Georgakoudi I. Osteoblastic differentiation and stress response of human mesenchymal stem cells exposed to alternating current electric fields. *Biomed Eng Online*. 2011;10(9):1-22. https://doi.org/10.1186/1475-925X-10-9.
15. Wu Y, Wang L, Guo B, Shao Y, Ma PX. Electroactive biodegradable polyurethane significantly enhanced Schwann cells myelin gene expression and neurotrophin secretion for peripheral nerve tissue engineering. *Biomaterials*. 2016;87:18-31. https://doi.org/10.1016/j.biomaterials.2016.02.010.
16. Qian Y, Zhao X, Han Q, Chen W, Li H, Yuan W. An integrated multilayer 3D-fabrication of PDA/RGD coated graphene loaded PCL nanoscaffold for peripheral nerve restoration. *Nat Commun*. 2018;9(1):323. https://doi.org/10.1038/s41467-017-02598-7.
17. Ghasemi-Mobarakeh L, Prabhakaran MP, Mohammad M, Nasr-Esfahani M, Baharvand H, Kiani S. Application of conductive polymers, scaffolds and electrical stimulation for nerve tissue engineering. *J Tissue Eng Regen Med*. 2011;5(4):e17-e35. https://doi.org/10.1016/j.progpolymsci.2018.01.001.
18. Guo B, Ma PX. Conducting Polymers for Tissue Engineering. *Biomacromolecules*. 2018;19(6):1764-1782. https://doi.org/10.1021/acs.biomac.8b00276.
19. Sun B, Wu T, Wang J, et al. Polypyrrole-coated poly(l-lactic acid-: Co -ε-caprolactone)/silk fibroin nanofibrous membranes promoting neural cell proliferation and differentiation with electrical stimulation. *J Mater Chem B*. 2016;4(41):6670-6679. https://doi.org/10.1039/c6tb01710j.
20. Lee JY, Bashur CA, Goldstein AS, Schmidt CE. Polypyrrole-coated electrospun PLGA nanofibers for neural tissue applications. *Biomaterials*. 2009;30(26):4325-4335. https://doi.org/10.1016/j.biomaterials.2009.04.042.
21. Huang Z, Guo Z, Sun M, Fang S, Li H. A study on graphene composites for peripheral nerve injury repair under electrical stimulation. *RSC Adv*. 2019;9(49):28627-28635. https://doi.org/10.1039/c9ra04855c.
22. Liu X, Li C, Pan Y, Schubert DW, Liu C. Shear-induced rheological and electrical properties of molten poly(methyl methacrylate)/carbon black nanocomposites. *Compos Part B Eng*. 2019;164:37-44. https://doi.org/10.1016/j.compositesb.2018.11.054.
23. Baranes K, Shevach M, Shefi O, Dvir T. Gold nanoparticle-decorated scaffolds promote neuronal differentiation and maturation. *Nano Lett*. 2016;16(5):2916-2920. https://doi.org/10.1021/acs.nanolett.5b04033.
24. Aydemir Sezer U, Ozturk K, Aru B, Yanıkkaya Demirel G, Sezer S, Bozkurt MR. Zero valent zinc nanoparticles promote neuroglial cell proliferation: a biodegradable and conductive filler candidate for nerve regeneration. *J Mater Sci Mater Med*. 2017;28(1):1-11. https://doi.org/10.1007/s10856-016-5831-1.
25. Tamboli MS, Palei PK, Patil SS, Kulkarni MV, Maldar NN, Kale BB. Polymethyl methacrylate (PMMA)–Bismuth Ferrite (BFO) nanocomposite: low loss and high dielectric constant materials with perceptible magnetic properties. *Dalt Trans*. 2014;43(35):13232-13241. https://doi.org/10.1039/b000000x.
26. Muneeswaran M, Jegatheesan P. Synthesis of nanosized BiFeO3 powders by co-precipitation method. *J Exp Nanosci*. 2013;8(3):341-346. https://doi.org/10.1080/17458080.2012.685954.
27. Yang SY, Zavaliche F, Mohaddes-Ardabili L, et al. Metalorganic chemical vapor deposition of lead-free ferroelectric BiFeO 3 films for memory applications. *Appl Phys Lett*. 2005;87(10):85-88. https://doi.org/10.1063/1.2041830.
28. Dash S, Choudhary RNP, Goswami MN. Enhanced dielectric and ferroelectric properties of PVDF-BiFeO3 composites in 0–3 connectivity. *J Alloys Compd*. 2017;715:29-36. https://doi.org/10.1016/j.jallcom.2017.04.310.
29. Ulag S, Kalkandelen C, Bedir T, Erdemir G, Erdem S. Fabrication of three-dimensional PCL/BiFeO3 scaffolds for biomedical applications. *Mater Sci Eng B*. 2020;261:114660. https://doi.org/10.1016/j.mseb.2020.114660.
30. Cores J, Caranasos T, Cheng K. Magnetically targeted stem cell delivery for regenerative medicine. *J Funct Biomater*. 2015;6(3):526-546. https://doi.org/10.3390/jfb6030526.
31. Ai J, Kiasat-Dolatabadi A, Ebrahimi-Barough S, et al. Polymeric scaffolds in neural tissue engineering: a review. *Arch Neurosci*. 2013;1(1):15-20. https://doi.org/10.5812/archneurosci.9144.

32. Hartono A, Satira S, Djamal M, Ramli R, Bahar H, Sanjaya E. Effect of mechanical treatment temperature on electrical properties and crystallite size of PVDF film. *Adv Mater Phys Chem*. 2013;03(01):71-76. https://doi.org/10.4236/ampc.2013.31011.
33. Vijayavenkataraman S, Thaharah S, Zhang S, Lu WF, Fuh JYH. 3D-printed PCL/rGO conductive scaffolds for peripheral nerve injury repair. *Artif Organs*. 2019;43(5):515-523. https://doi.org/10.1111/aor.13360.
34. Adams SD, Ashok A, Kanwar RK, Kanwar JR, Kouzani AZ. Integrated 3D printed scaffolds and electrical stimulation for enhancing primary human cardiomyocyte cultures. *Bioprinting*. 2017;6:18-24. https://doi.org/10.1016/j.bprint.2017.04.003.
35. Aydin C, Aydin H, Taskin M. Low-temperature synthesis and characterization of bismuth ferrite/graphene oxide nano electroceramics by the hydrothermal method. *J Phys Chem Funct Mater*. 2018;1(1):102-116.
36. She Y, Luo W, Zhu L, Wang N, Tang H, Cao M. Efficient removal of organic pollutants with magnetic nanoscaled BiFeO 3 as a reusable heterogeneous fenton-like catalyst. *Environ Sci Technol*. 2010;44(5):1786-1791.
37. Pandele AM, Constantinescu A, Radu IC, Miculescu F, Voicu SI, Ciocan LT. Synthesis and characterization of PLA-micro-structured hydroxyapatite composite films. *Materials (Basel)*. 2020;13(2):1-13.
38. Mikhailov AV, Gribchenkova NA, Kolosov EN, Kaul AR, Alikhanyan AS. Mass spectrometric investigation of vaporization in the Bi2O3–Fe2O3 system. *Chem Thermodyn Thermochem Mass*. 2011;85(1):31-35. https://doi.org/10.1134/S0036024411010183.
39. Sakar M, Balakumar S, Saravanan P, Jaisankar SN. Annealing temperature mediated physical properties of bismuth ferrite (BiFeO3) nanostructures synthesized by a novel wet chemical method. *Mater Res Bull*. 2013;48(8):2878-2885. https://doi.org/10.1016/j.materresbull.2013.04.008.
40. Chieng BW, Ibrahim NA, Then YY, Loo YY. Epoxidized vegetable oils plasticized poly(lactic acid) biocomposites: mechanical, thermal and morphology properties. *Molecules*. 2014;19:16024-16038. https://doi.org/10.3390/molecules191016024.
41. Zhang H, Huang J, Yang L, et al. Preparation, characterization and properties of PLA/TiO2 nanocomposites based on a novel vane extruder. *RSC Adv*. 2015;5(6):4639-4647. https://doi.org/10.1039/c4ra14538k.
42. Srivastav SK, Gajbhiye NS. Low temperature synthesis, structural, optical and magnetic properties of bismuth ferrite nanoparticles. *J Am Ceram Soc*. 2012;95(11):3678-3682. https://doi.org/10.1111/j.1551-2916.2012.05411.x.
43. Godara S, Sinha N, Ray G, Kumar B. Combined structural, electrical, magnetic and optical characterization of bismuth ferrite nanoparticles synthesized by auto-combustion route. *J Asian Ceram Soc*. 2014;2(4):416-421. https://doi.org/10.1016/j.jascer.2014.09.001.
44. Jia DC, Xu JH, Ke H, Wang W, Zhou Y. Structure and multiferroic properties of BiFeO3 powders. *J Eur Ceram Soc*. 2009;29(14):3099-3103. https://doi.org/10.1016/j.jeurceramsoc.2009.04.023.
45. Puchalski M, Kwolek S, Szparaga G, Chrzanowski M. Investigation of the influence of PLA molecular structure on the crystalline forms (α' and α) and mechanical properties of wet spinning fibres. *Polymers (Basel)*. 2017;9(18):1-13. https://doi.org/10.3390/polym9010018.
46. Jia S, Yu D, Zhu Y, Wang Z, Chen L, Fu L. Morphology, crystallization and thermal behaviors of PLA-based composites: wonderful effects of hybrid GO/PEG via dynamic impregnating. *Polymers (Basel)*. 2017;9(528):1-18. https://doi.org/10.3390/polym9100528.
47. Farid T, Herrera VN, Kristiina O. Investigation of crystalline structure of plasticized poly(lactic acid)/ Banana nanofibers composites Investigation of crystalline structure of plasticized poly (lactic acid)/Banana nanofibers composites. *Mater Sci Eng*. 2018;369:012031. https://doi.org/10.1088/1757-899X/369/1/012031.
48. Zakaria Z, Islam MS, Hassan A, et al. Mechanical properties and morphological characterization of PLA/chitosan/epoxidized natural rubber composites. *Adv Mater Sci Eng*. 2013;2013:7. https://doi.org/10.1155/2013/629092.
49. Mishra MK, Moharana S, Behera B, Mahaling RN. Surface functionalization of BiFeO3: a pathway for the enhancement of dielectric and electrical properties of poly(methyl methacrylate)–BiFeO3 composite films. *Front Mater Sci*. 2017;11(1):82-91. https://doi.org/10.1007/s11706-017-0364-1.
50. Dominici M, Le Blanc K, Mueller I, et al. Minimal criteria for defining multipotent mesenchymal stromal cells. The international society for cellular therapy position statement. *Cytotherapy*. 2006;8(4):315-317. https://doi.org/10.1080/14653240600855905.
51. Intaraprasit S, Faikrua A, Sittichokechaiwut A, Viyoch J. Efficacy evaluation of the fibroblast-seeded collagen/chitosan scaffold on application in skin tissue engineering. *ScienceAsia*. 2012;38(3):268-277. https://doi.org/10.2306/scienceasia1513-1874.2012.38.268.
52. Gregor A, Filová E, Novák M, et al. Designing of PLA scaffolds for bone tissue replacement fabricated by ordinary commercial 3D printer. *J Biol Eng*. 2017;11(1):31. https://doi.org/10.1186/s13036-017-0074-3.
53. Ferrari M, Cirisano F, Morán MC. Mammalian cell behavior on hydrophobic substrates: influence of surface properties. *Colloids Interfaces*. 2019;3(2):48. https://doi.org/10.3390/colloids3020048.
54. Alksne M, Simoliunas E, Kalvaityte M, et al. The effect of larger than cell diameter polylactic acid surface patterns on osteogenic differentiation of rat dental pulp stem cells. *J Biomed Mater Res Part A*. 2018;9999:1-13. https://doi.org/10.1002/jbm.a.36547.
55. Heo SJ, Szczesny SE, Kim DH, Saleh KS, Mauck RL. Expansion of mesenchymal stem cells on electrospun scaffolds maintains stemness, mechano-responsivity, and differentiation potential. *J Orthop Res*. 2018;36(2):808-815. https://doi.org/10.1002/jor.23772.
56. Dennaoui H, Chouery E, Rammal H, Abdel-Razzak Z, Harmouch C. Chitosan/hyaluronic acid multilayer films are biocompatible substrate for wharton's jelly derived stem cells. *Stem Cell Investig*. 2018;5(47):1-8. https://doi.org/10.21037/sci.2018.12.02.
57. Chatzinikolaidou M, Rekstyte S, Danilevicius P, et al. Adhesion and growth of human bone marrow mesenchymal stem cells on precise-geometry 3D organic-inorganic composite scaffolds for bone repair. *Mater Sci Eng C*. 2015;48:301-309. https://doi.org/10.1016/j.msec.2014.12.007.
58. Shi S, Gronthos S. Bone marrow mesenchymal stem cells. In: *Stem Cells in Craniofacial Development and Regeneration*. 2013;223-239. https://doi.org/10.1002/9781118498026.ch11.
59. Banks TA, Luckman P, Frith JE, Cooper-White JJ. Effects of electric fields on human mesenchymal stem cell behaviour and morphology using a novel multichannel device. *Integr Biol*. 2015;7(6):693-712. https://doi.org/10.1039/c4ib00297k.
60. Shao S, Zhou S, Li L, et al. Osteoblast function on electrically conductive electrospun PLA/MWCNTs nanofibers. *Biomaterials*. 2011;32(11):2821-2833. https://doi.org/10.1016/j.biomaterials.2011.01.051.
61. Ko UH, Park S, Bang H, Kim M, Shin H, Shin JH. Promotion of myogenic maturation by timely application of electric field along the topographical alignment. *Tissue Eng-Part A*. 2018;24(9–10):752-760. https://doi.org/10.1089/ten.tea.2017.0055.

SUPPORTING INFORMATION

Additional supporting information may be found online in the Supporting Information section at the end of this article.

How to cite this article: Bedir T, Ulag S, Aydogan K, et al. Effect of electric stimulus on human adipose-derived mesenchymal stem cells cultured in 3D-printed scaffolds. *Polym Adv Technol*. 2021;32:1114–1125. https://doi.org/10.1002/pat.5159